Meteorol. Z. (Contrib. Atm. Sci.), Vol. **29**, No. 5, 393–407 (published online July 14, 2020)

Characteristics of deep moist convection over Germany in multi-source data

Isabella Zöbisch[1*], Caroline Forster[1], Tobias Zinner[2], Luca Bugliaro[1], Arnold Tafferner[1] and Kathrin Wapler[3]

[1]Deutsches Zentrum für Luft- und Raumfahrt, Institut für Physik der Atmosphäre, Oberpfaffenhofen, Germany
[2]Meteorologisches Institut, Ludwig-Maximilians-Universität München, Munich, Germany
[3]Deutscher Wetterdienst, Offenbach, Germany

(Manuscript received December 6, 2019; in revised form May 14, 2020; accepted May 14, 2020)

Abstract

This study analyses characteristics of deep moist convection (DMC) over Germany with the aim to select relevant parameters that have the skill to improve the identification of current life cycle phase and the forecast of a lifetime of DMCs in an operational weather forecasting environment. No differentiation between thunderstorm organization types is done, since no simple differentiation method is available in an operational environment. In contrast to previous analyses, multiple data sources are used synchronously to explore an extensive data set of DMCs at high resolution in space and time. Basis of our analysis are all DMC detections in satellite data (using Cb-TRAM – Thunderstorm Tracking and Monitoring) in a five month period (June 2016, May/June/July 2017, and June 2018). For each of these DMCs the time series of selected parameters from satellite, ground-based radar, lightning detection, and numerical weather prediction (NWP) model data are inspected. In search for clear signatures of expectable lifetime and differences between short- and long-lived DMCs, all thunderstorm systems are sorted by their lifetime. In addition, they are separated into four life cycle phases: 1. *early growth*, 2. *advanced growth*, 3. *maturity*, and 4. *decay*. Generally, it turns out that satellite, radar, and lightning data are the most suitable data to determine the actual life cycle phase of a DMC. It is shown that long-lived DMCs are, on average, related to lower minimum cloud top temperature and mid-level relative humidity and higher maximum of coverage area, vertically integrated water and lightning activity during their life cycle than short-lived systems. The NWP model parameters have a diagnostic potential to identify the remaining lifetime in connection with the observational data, but do not contain information about the actual life cycle phase. The results obtained in this study will be used for an investigation of their potential application in a nowcasting model, in order to determine the current phase of an observed DMC and to predict its remaining lifetime.

Keywords: thunderstorms, lifetime characteristics, multi-source, Germany

1 Introduction

Thunderstorms are most frequent and generally most intensive over Germany during the summer months (e.g. Wapler, 2013; Taszarek et al., 2019). Severe thunderstorms have high impact on society and safety (Brooks and Dotzek, 2008). Therefore, thunderstorm observation and analysis started a long time ago. The first model describing the life cycle of a single thunderstorm cell was presented by Byers and Braham Jr. (1948). They separated the life cycle on the basis of observations (in particular aircraft data) into three stages: growing, mature, and dissipation. The stages were characterized and defined by wind field and microphysics. In the following, we provide a summary of a variety of selected thunderstorm studies based on satellite, radar, lightning, or model data, without claiming to provide a complete literature review.

Several studies analyzed parameters from satellite, radar, lightning, and NWP model data to identify correlations to the thunderstorm's lifetime (e.g. Machado et al., 1997) or typical signatures in the life cycle (e.g. Mecikalski et al., 2011; Mecikalski et al., 2016). In the first half of the life cycle, an isolated cumulus cloud growing in a clear sky shows an increasing optical thickness and cloud top effective radius until the cloud top glaciates and a decreasing of the effective radius is initiated (Mecikalski et al., 2011). Besides cloud top glaciation, an increased updraft leads to smaller ice particles because of reduced growing time and additional activation of new particles (Setvák and Doswell, 1991; Rosenfeld et al., 2008; Senf and Deneke, 2017). This increased updraft that is described by large cloud-top cooling rates can be detected 30 min before radar reflectivities of minimum 35 dBZ are measured (Roberts and Rutledge, 2003). High cloud-top-cooling rates in the early phases of a thunderstorm are associated with hail occurrence later in the life cycle (Hartung et al., 2013). A cumulus cloud showing a rainfall of 35 dBZ in its early phase will most likely

*Corresponding author: Isabella Zöbisch, Deutsches Zentrum für Luft- und Raumfahrt, Institut für Physik der Atmosphäre, Münchener Straße 20, 82234 Weßling, Germany, e-mail: isabella.zoebisch@dlr.de

DOI 10.1127/metz/2020/1011

Gebrüder Borntraeger Science Publishers, Stuttgart, www.borntraeger-cramer.com

develop into a mature cumulonimbus cloud (Roberts and Rutledge, 2003). In the late first half of the life cycle, the maximum reflectivity is observed (Davini et al., 2012). High lightning activity can be detected slightly before an overshooting top occurs (Jurković et al., 2015). The mature stage is characterized by regions of strong vertical motion advecting ice hydrometeors into the upper troposphere and lower stratosphere (Mecikalski et al., 2012). During the maturation of a thunderstorm its maximum of the lightning occurrence can be detected (Mattos and Machado, 2011; Rigo et al., 2010). Additionally, Mattos and Machado (2011) described a strong correlation of lightning occurrence with vertically integrated ice content and particle size. A correlation of the maximum cloud top height, maximum precipitation intensity, and core size was shown by Senf and Deneke (2017) for thunderstorms over Europe.

The lifetime of a thunderstorm correlates with its coverage area (Machado et al., 1997; Mathon and Laurent, 2001; Feng et al., 2012), whereas no differences between short- and long-lived thunderstorms exist for the brightness temperature temporal changes (Machado et al., 1997). The positive correlation of lifetime and size was analyzed for thunderstorms over the Americas (tropical and mid latitude) (Machado et al., 1997) and over the Sahelian zone (Mathon and Laurent, 2001). Although no correlation between lifetime and temperature temporal changes were reported, Hartung et al. (2013) showed that strong cloud top cooling rates (associated with an intense vertical growth) correlate with intense precipitation rates. A positive correlation of maximum reflectivity and lifetime was analyzed for thunderstorms over Italy (Davini et al., 2012) and Germany (Wapler, submitted). The lifetime also correlates positively with the lightning occurrence for thunderstorms over Spain (Rigo et al., 2010) and Germany (Wapler, submitted). A sudden increase in lightning activity (lightning jump) is an indicator for intense thunderstorms (e.g. Schultz et al., 2009; Schultz et al., 2011; Farnell et al., 2017; Wapler, 2017). Severe thunderstorms show a quicker horizontal growth than non-severe storms (Cintineo et al., 2013). Hagen and Finke (1999) investigated thunderstorms (divided into organization types) over southern Germany and found that Convective Available Potential Energy (CAPE) on average ranged between about 600 and 900 $\mathrm{J\,kg^{-1}}$ related to their motion and type of organization. Taszarek et al. (2019) performed analysis for severe weather events over Europe and showed that thunderstorms occur, if CAPE is greater than 150 $\mathrm{J\,kg^{-1}}$. CAPE can also be related to the maximum updraft velocity according to Emanuel (1994).

On the one hand, numerical weather forecast models can calculate the atmospheric state hours and days in advance. Nonetheless, individual thunderstorm cells' occurrence and lifetime are not predictable due to the statistical nature of the involved processes, the lack of detailed observations to describe the initial state for these turbulent developments, and the limited spatial resolution of the model. On the other hand, observations from satellite and weather radar enable the exact detection of existing thunderstorms, but do only allow a nowcast based on the extrapolation of the observations which is valid for a very limited time period. An overview of the current nowcasting systems is given in the nowcasting guidelines published by WMO (Wang et al., 2017). Some of the existing nowcasting systems already focus on the tracking and nowcasting of particular organization types or life cycle phases. Examples are Tracking Of Organized Convection Algorithm through a 3-D segmentatioN (TOOCAN) (Fiolleau and Roca, 2013) which focuses on MCS, the EUMETSAT Nowcasting Satellite Application Facility's Rapidly Developing Thunderstorm (RDT) algorithm (Guillou, 2010) and the algorithm by Mecikalski and Bedka (2006) with a focus on the convective initiation stage. Additionally, there exist nowcasting systems based on multi source data. Examples are the Context and Scale Oriented Thunderstorm Satellite Predictors Development (COALITION) (Nisi et al., 2014), NowCastMIX (James et al., 2018) and "probsevere" (Cintineo et al., 2018). However, the nowcasting beyond one hour quickly becomes inaccurate (Sun et al., 2014). It fails when it comes to the prediction of the remaining lifetime, since the extrapolation is just based on motion and intensity seen at the time of analysis in the history of available data fields, and no physical processes are taken into account.

The previously referenced studies are based on analyses of specific historical data bases and focus on specific aspects of selected organization types or thunderstorm development stages. However, when it comes to weather forecasting the operationally available data and tools described previously do neither provide reliable information on the organization type nor the current life cycle phase of an observed thunderstorm. Usually, only general environmental information is available from an operational numerical weather forecast as well as information from observation based nowcasting of an indiscriminate mixture of thunderstorm systems of all types. Therefore, the challenge is the improvement of predictions of the remaining lifetime of existing thunderstorms in an operational environment, regardless of their organization type. The present study describes the first step necessary to develop such a method. We intend to find relevant parameters with observable characteristics related to lifetime, like the size of long-lived thunderstorms as in Machado et al. (1997), which are valid for a broad spectrum of DMCs with predictive skill for a forecast of lifetime of any kind of DMC.

The study is structured as follows: Section 2 introduces the different data sources and the treatment of the used parameters as well as a description of Cb-TRAM. Section 3 presents the typical characteristics of the available data during the observed life cycle of thunderstorms detected by Cb-TRAM (Cb-TRAM thunderstorm objects). The new findings and the conclusions drawn are

Table 1: All parameters explored for typical signatures over the lifetime of DMCs as detected by Cb-TRAM.

Data source	Parameter	Abbrev.	Unit
Satellite	brightness temperature	*BT*	K
	cloud optical thickness	τ	–
	effective radius	r_e	µm
	ice fraction at the cloud top	*ice fraction*	%
	area inside A_{cb} where $\tau > 0.1$	$A_{\tau>0.1}$	km^2
Cb-TRAM	area of the Cb-TRAM cell	A_{cb}	km^2
Radar	vertically integrated ice content	*VII*	$kg\,m^{-2}$
	vertically integrated liquid water content	*VIL*	$kg\,m^{-2}$
Rad-TRAM	area of the 46 dBZ contour	RA_{46}	km^2
	maximum reflectivity	R_{max}	dBZ
LINET	lightning detection during 5 min	*Li*	$\#\,5\,min^{-1}$
COSMO-DE	mixed layer Convective Available Potential Energy	*CAPE*	$J\,kg^{-1}$
	relative humidity at 700 hPa	*RH*	%
	vertical velocity at 700 hPa	ω	$Pa\,s^{-1}$

summarized in Section 4. Note that when we speak about "thunderstorms" or "DMCs" in the following, we always mean all kinds of organziation types like MCS, multicells, supercells and single cells. Similarly, when we use the term "life cycle" we always mean an average life cycle over a multitude of different organization types. To categorize the broad spectrum of data sources and corresponding available parameters, the following questions are investigated:

1. Which parameters contain redundant information on the life cycle?

2. Which parameters are able to describe certain life cycle phases, and what are their typical characteristics throughout each life cycle phases?

3. Are there differences in the life cycle between long-lived and short-lived thunderstorms?

4. Why do some parameters not contain any information on the life cycle phase?

2 Data and methods

The basis for this study is a satellite-based detection of thunderstorms provided by the Cb-TRAM algorithm (Zinner et al., 2008; Zinner et al., 2013,). In addition, data from radar, lightning detection network, satellite, and numerical weather forecasts are used to explore all Cb-TRAM detections over Germany for the period June 2016, May, June, and July 2017, and June 2018 in order to find a set of parameters showing signatures of lifetime stage and remaining lifetime. In the following, the thunderstorm definition and the parameters are described in detail. A summary of all data sources and examined parameters is presented in Table 1.

2.1 Geostationary satellite data

Data from the rapid scanning mode of "The Spinning Enhanced Visible and Infra-Red Imager" (SEVIRI) aboard the geostationary Meteosat Second Generation satellite (MSG, Schmetz et al., 2002) is used to determine the satellite parameters and to detect the thunderstorms.

2.1.1 Cloud properties

The visible (VIS) and infrared (IR) channels are used to determine the parameters cloud optical thickness (τ), effective radius (r_e), ice fraction at the cloud top (*ice fraction*), and brightness temperature (*BT*) at 10.8 µm with the "Algorithm for the Physical Investigation of Clouds with SEVIRI" (APICS, Bugliaro et al., 2011) and the "cirrus optical properties derived from CALIOP and SEVIRI algorithm during day and night" algorithm (COCS, Kox et al., 2014). The data has a temporal resolution of 5 minutes and a spatial resolution of 3 km × 3 km at the sub-satellite point (point where the line between satellite and the center of the Earth intersects the Earth's surface). Values of 100 % for *ice fraction* indicate a thunderstorm cloud top completely covered with ice particles, values of 0 a pure liquid cloud top. The parameter *BT* is derived from measurements in the IR 10.8 µm window channel and the black-body assumption. The parameters τ and r_e are calculated using observations from two channels (0.75 and 2.16 µm) comparable to Nakajima and King (1990). Measurement accuracy limits the retrieved values of τ to a maximum of 100. Although theoretical optical thickness up to 1000 is realistic for convective clouds, observable cloud brightness is hardly changed above the limit anymore. The parameter r_e is the measure of cloud particle size determinable by remote sensing. Most of the time, it is closely related to the mean for a mono-modal Gamma size distribution (Hansen and Travis, 1974).

2.1.2 Thunderstorm detection

In this study a thunderstorm is defined as an object identified in MSG rapid scanning satellite data by the CumulonimBus TRacking And Monitoring (Cb-TRAM). This is an algorithm that detects, tracks, and nowcasts deep DMCs without differentiation between organization types (Zinner et al., 2008; Zinner et al., 2013). Three different warning levels, comparable to life cycle stages, are distinguished by Cb-TRAM using two IR, one water vapor (WV), and the high-resolution visible (HRV) channels. Convective objects that belong to the Cb-TRAM warning level "early development" show strong vertical and/or horizontal growth indicated by rapid cooling in the IR 10.8 µm channel and a significant increase in the HRV reflectivity. The Cb-TRAM warning level "rapid development" is detected through a strong cooling in the WV 6.2 µm channel, and the level "mature thunderstorm" is determined using a difference of WV 6.2 µm and IR 10.8 µm and a strong local texture in the HRV channel.

Figure 1 (center) shows an example of a Cb-TRAM cell encompassing a multi-cell (red contour). The regions of increased roughness (strong local texture in the HRV channel) indicate the different regions of strong convection inside the Cb-TRAM cell. As shown in the figure the cell consists of several updraft regions. The 60 min nowcast (red dashed contour) indicates a relatively steady thunderstorm (moving speed about 15 m/s), since the contours of the detection and the nowcast overlap for the most part. Based on an image matching algorithm, a displacement vector field is derived and used to track each thunderstorm in time (Zinner et al., 2008). A forward-extrapolation of all object positions for 60 minutes after the current detection provides Cb-TRAM's nowcast (Zinner et al., 2008). In the following study one of these nowcasts is used to extend the analyzable part of the life cycle following the last detection. As Cb-TRAM focuses on active thunderstorms, the usually undetected decay can be included into the analysis this way. In a similar way, the displacement vector field is used to extend the analyzable part of the life-cycle onto the 30 minutes before the first detection. To this end a backward-extrapolation of all object positions is applied (inverting the sign of the extrapolation). The coverage in time and space provided by our basic object definition is extended this way. This will allow a more complete analysis of observational signals during otherwise excluded parts of convective initiation and dissipation.

As especially these extensions carry considerable uncertainty regarding cloud cover, the following analyses only considers the area within a Cb-TRAM object where τ is greater than 0 ($A_{\tau>0.1}$). That means, the life cycle of a Cb-TRAM detected thunderstorm starts as soon as $A_{\tau>0.1}$ is greater than 0 and ends when $A_{\tau>0.1}$ is equal to 0 again. Since the τ is derived from visible channel information, only thunderstorms occurring in the daytime are considered in the life cycle analysis. In order to enable the comparison of Cb-TRAM detections with other measurement data, the parallax shift due to the satellite viewing angle is corrected using a constant cloud top height of 10 km.

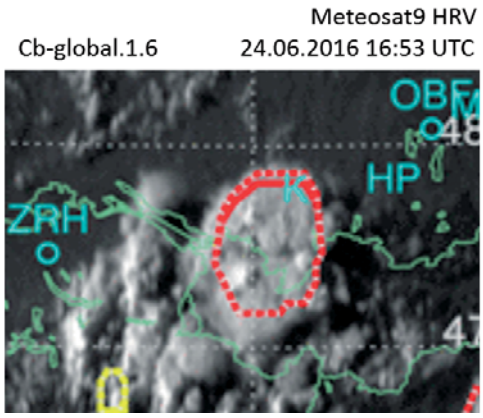

Figure 1: Example for Cb-TRAM detections. Red contours show detections assigned to warning level "mature thunderstorm" (red dashed contours show the 60 min nowcast). Yellow contours indicate warning level "early development".

2.2 Radar data

The German Weather Service (Deutscher Wetterdienst, DWD) operates a network of 17 polarimetric Doppler C-Band radar systems (Helmert et al., 2014) over Germany (see Figure 2). Parameters from the precipitation scan and additional parameters from the volume scan are used in this analyses.

2.2.1 Volume scan

Each of the radar provides a new volume scan every 5 min with a horizontal radius of up to 180 km and a vertical extent from surface near layers to the upper troposphere (about 10 km height). The intensity of precipitation is categorized into 255 classes. The DWD 3D radar products reflectivity vertically integrated ice content (*VII*) and vertically integrated liquid water content (*VIL*) are analyzed over the life cycle of thunderstorms. For a detailed description of *VII* and *VIL* calculation see Greene and Clark (1972).

2.2.2 Precipitation scan

Beside the volume scan a precipitation scan is used for the life cycle analyses as a measure of precipitation. For these scans the radar elevation angle is "terrain following" (elevation angle dependent on orography). An algorithm that uses the precipitation scan to detect, track, and nowcast precipitation cells is "Radar TRacking And Monitoring" (Rad-TRAM, Kober and Tafferner, 2009). Rad-TRAM cells are output for six different reflectivity thresholds: 19, 28, 37, 46, 55, and 64 dBZ. The average of the highest 30 % of all reflectivity values within the 19 dBZ Rad-TRAM cell (maximum reflectivity ($R_{\max}$)) and the area of the 46 dBZ contour

(RA_{46}) are used for the analyses in this study, whenever a 19 dBZ or 46 dBZ Rad-TRAM cell overlaps with a Cb-TRAM object. The parameter R_{max} is selected to determine the typical maximal reflectivity of a thunderstorm. The parameter RA_{46} has been chosen, because the 46 dBZ threshold is an indicator for very heavy rain and possible hail (Waldvogel et al., 1979).

2.3 Lightning data

Data of the "European ground-based LIghtning NETwork" (LINET) from nowcast GmbH (Betz et al., 2009) with a statistical average accuracy of approximately 150 m is used in this study. With the very low frequency (3–30 KHz) and low frequency (30–300 kHz) lightning detection technique, it is possible to measure cloud-to-ground (CG) and cloud-to-cloud (IC) lightning. In the following life cycle analysis both lightning categories are considered together. All lightning (CG and IC) observations that occur 2.5 min before and 2.5 min after the Cb-TRAM detection inside a Cb-TRAM object are accumulated. The resulting parameter is called lightning detection (*Li*).

2.4 COSMO-DE Model

The Consortium for Small-Scale Modeling (COSMO) was formed in 1998. The numerical weather prediction (NWP) model COSMO-DE has been operated at the DWD (Baldauf et al., 2006) since January of 2007. The COSMO-DE model has a spatial resolution of 2.8 km × 2.8 km. It has a hybrid terrain-following vertical coordinate separated in 50 model layers with the lowest at 0 m above the surface and the highest at 22 km absolute altitude. The levels are constant over time. The domain covers Germany, Austria, and Switzerland with 421x461 data points (see Figure 2). In May 2018 COSMO-DE was replaced by COSMO-D2 with a higher spatial resolution (2.2 km x 2.2 km) and 65 layers. This setup is used for a part of the period (June 2018) analyzed in this study (see Section 2.5). The update cycle of both COSMO-DE and COSMO-D2 is 3 hours (00, 03, 06, 09, 12, 15, 18, and 21 UTC). Forecasts are output with an interval of 1 hour until 21 hours. For further analysis these are interpolated to a temporal resolution of 5 min to be able to compare model parameters to observations. For the life cycle analyses the latest available forecast relative to the observation time of thunderstorms is used. For example, the 2 h forecast of the 06 UTC run is used for a thunderstorm detected at 8 UTC. The parameters *CAPE*, relative humidity at 700 hPa (*RH*), and vertical velocity at 700 hPa (ω) are used for the analysis in this study, since they are an indicator for instability (*CAPE*), moist energy for thunderstorm development (*RH*) and modelled updraft speed (ω). Their predictive skill for thunderstorm occurrence and intensity was verified by several studies (e.g. Kuligowski and Barros, 1998; Benjamin et al., 2004; Kaltenböck et al., 2009; Kahraman et al., 2017). *RH* and ω are picked from a level of 700 hPa, due to their predictive skill for thunderstorm lifetime at this level following, for example, in Kuligowski and Barros (1998) or Benjamin et al. (2004).

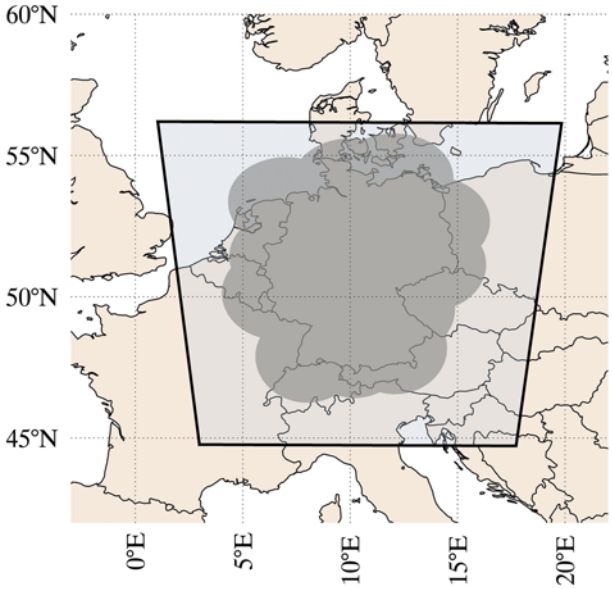

Figure 2: Map of Central Europe with coverage of COSMO-DE data (rectangular light grey shaded area) and the coverage of the DWD radar network (dark grey shaded area).

2.5 Data fusion

Table 1 summarizes all parameters analyzed for this study. The operational availability of every parameter for every analyzed storm object is important for an optimal operationally applicable thunderstorm nowcasting. Consequently every thunderstorm is considered, if it occurs inside the DWD radar network coverage (Figure 2) and shows a "mature-thunderstorm" detection by Cb-TRAM at least for one time step during the lifetime of the Cb-TRAM object.

For the analysis minimum brightness temperature (BT_{min}) as well as τ, r_e, and *ice fraction* are calculated. In order to focus on the most active regions and to reduce the influence of outliers, these are generated by averaging over the 10 % of the pixels with the lowest *BT* values inside area of the Cb-TRAM cell (A_{cb}). The radar parameters maximum vertically integrated ice content (VII_{max}) and maximum vertically integrated liquid water content (VIL_{max}) are the average of the highest 10 % of all *VII* and *VII* values within a thunderstorm. Finally, information on the convective environment is collected over a model grid box with 50 km radius around the thunderstorm object, in order to smooth variability which is high in the model atmosphere in convective situations. This way, effects of convective cell location in the model and their differences to observed positions are minimized. The parameters Convective Available Potential Energy ($CAPE_{max}$) and minimum vertical

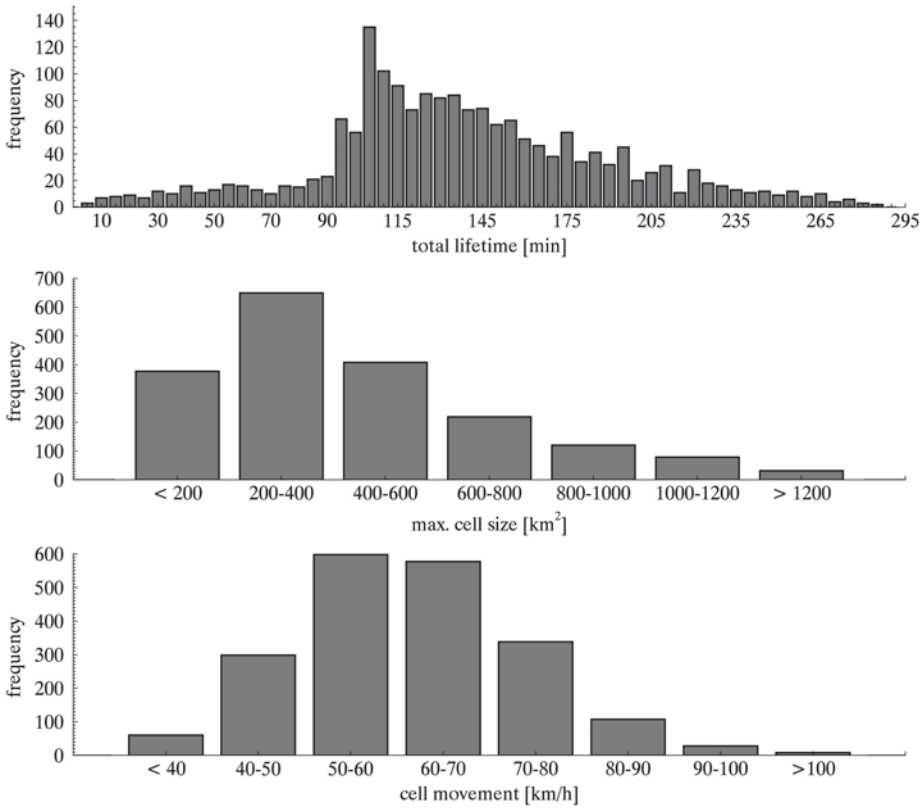

Figure 3: Frequency of thunderstorms with different total lifetimes, maximum cell sizes and mean cell movement over Germany in June of 2016; May, June, July of 2017; and June of 2018.

velocity at 700 hPa (ω_{min}) are determined by the average over 10 % highest Convective Available Potential Energy (*CAPE*) and 10 % most negative ω values (the strongest updrafts) within each 50 km radius. The parameter *RH* is an average over all *RH* values within each 50 km radius.

3 Life cycle of thunderstorm properties

3.1 Lifetime frequency based on satellite data

Almost 1900 thunderstorms with lifetimes between 5 and 300 minutes have been detected with Cb-TRAM within the coverage of the DWD radar network in June 2016, May, June, and July 2017, and June 2018 (Figure 3, top). More than half of all detected thunderstorms have a total lifetime between 90 and 175 mins. Thunderstorms that exist longer than 300 min occur very rarely, since the detection area is limited to Germany. There the main track directory is south-west and Germany has a geographical extend of approximately 850×600 km^2 (N–S × W–E). Short-lived thunderstorms (<90 min) occur rarely. Most of the thunderstorms have a maximum cell size between 200–400 km^2 during their life cycle (Figure 3, middle). The mean propagation speed detected during the thunderstorms life cycle is between 50–60 km/h for the most thunderstorms (Figure 3, bottom). It should be noted that the frequency distribution of the lifetime differs from the usual definition of individual thunderstorms. There lifetimes below 60 min show the highest frequency (e.g. in Wilson et al., 1998; Meyer et al., 2013). In contrast to theses studies, the life cycle analyses presented in the following includes all developments whenever they can be separated from background in satellite data. This includes the possibility that start or end of the convective development is hidden by other clouds. This is a possible explanation for the low frequency of lifetimes below 90 min, since they never reach heights greater than the overlaying cloud cover and, therefore, were not detected. To avoid these incomplete life cycles due to satellite detection, previous studies concentrated on selected isolated thunderstorms (e.g. Mecikalski et al., 2011) or analyzed the period around a certain event, for example, the maximum cooling rate as in Senf et al. (2015). In the following analysis no additional life cycle criterion is used, because the focus of this study is to determine parameters suitable for lifetime prediction of thunderstorms detected operationally by the satellite-based detection method Cb-TRAM. Therefore all thunderstorms detected by Cb-TRAM (with complete and incomplete life cycles) will be considered. In general, the lifetime frequency distribution is closely related to the detection method and definition of a thunderstorm (e.g., until the anvil completely dissolved as in Strandgren and

Table 2: *Linear Pearson Correlation Coefficients (r)* of the averaged life cycles of all thunderstorms normalized to one lifetime progress for all the parameters from satellite, radar, lightning, and model data.

	A_{cb}	$A_{\tau>0.1}$	$BT_{\min}$	τ	r_e	*ice fraction*	$R_{\max}$	RA_{46}	$VII_{\max}$	$VIL_{\max}$	*Li*
A_{cb}	1	0.99	−0.89	0.7	−0.66	0.8	0.05	0.59	0.1	−0.4	0.8
$A_{\tau>0.1}$	0.99	1	−0.88	0.68	−0.69	0.77	0.03	0.54	0.05	−0.08	0.79
$BT_{\min}$	−0.89	−0.88	1	−0.85	0.38	−0.9	−0.31	−0.7	−0.37	−0.24	−0.86
τ	0.7	0.68	−0.85	1	−0.04	0.69	0.7	0.87	0.7	0.6	0.89
r_e	−0.66	−0.69	0.38	−0.04	1	−0.41	0.56	0.1	0.59	0.68	−0.17
ice fraction	0.8	0.77	−0.9	0.69	−0.41	1	0.02	0.4	0.1	0	0.59
$R_{\max}$	0.05	0.03	−0.31	0.7	.0.56	0.02	1	0.76	0.93	0.95	0.58
RA_{46}	0.59	0.54	−0.7	0.87	0.1	0.4	0.76	1	0.83	0.76	0.94
$VII_{\max}$	0.1	0.05	−0.37	0.7	0.59	0.1	0.93	0.83	1	0.98	0.66
$VIL_{\max}$	−0.4	−0.08	−0.24	0.6	0.68	0	0.95	0.76	0.98	1	0.54
Li	0.8	0.79	−0.86	0.89	−0.17	0.59	0.58	0.94	0.66	0.54	1

Bugliaro (2018) or until strong updrafts cease as assumed in Zinner et al. (2008).

In order to compare the specific characteristics of each life cycle phase independent of the individual lifetime of Cb-TRAM objects, the thunderstorm lifetimes are normalized to a lifetime progress 0–100 % and categorized into the lifetime classes short-lived (5–90 min, 260 cases), medium-lived (95–180 min, 1268 cases) and long-lived (185–300 min, 331 cases).

3.2 Parameter selection

Some parameters of the same data source show similar characteristics over the life cycle and contain redundant information. Therefore, the *Linear Pearson Correlation Coefficient* has been calculated for all parameters (see Table 2). Only one of the parameters for each data source is selected for further study, if it shows similar evolution over the life cycle. The temporal changes over the life cycle of the parameters $VII_{\max}$ and $VIL_{\max}$ correlate very well. The same is the case for $R_{\max}$ and RA_{46}. Therefore the parameters $VIL_{\max}$ and $R_{\max}$ are selected to describe the life cycle in radar data, one from volume and one from precipitation scans. With regard to the satellite data, the parameters $A_{\tau>0.1}$, τ, r_e, *ice fraction*, and $BT_{\min}$ have been selected. Model parameters are treated separately in Section 3.4, because of their ability to provide non-local environmental information.

3.3 The life cycle in observational data

The aim of this section is to gain information about average life cycle phases (represented by the average life cycle of thunderstorms with lifetimes between 95–180 min) and about differences between the life cycles of long- (185–300 min) and short-lived (5–90 min) storm objects. Each life cycle phase is analyzed separately using the selected parameters: $BT_{\min}$, $A_{\tau>0.1}$, τ, r_e, *ice fraction*, $R_{\max}$, $VIL_{\max}$ and *Li*.

For the life cycle analyses all thunderstorms of each lifetime class are averaged over their normalized lifetime. The lifetime class comprising thunderstorms with lifetimes of 5–90 min is classified as short-lived and that with lifetimes of 185–300 min is classified as long-lived. It has to be considered that short-lived and long-lived Cb-TRAM objects are rare and very short-lived objects (lifetimes less than 15 min) do not cover every life cycle phase. Consequently, the life cycle of these two categories is probably influenced by outliers. The lifetime class that includes thunderstorms with lifetimes of 95–180 min is categorized here as "medium-lived", since most of the thunderstorms analyzed in this study have lifetimes in this range. This lifetime class is used to describe the general life cycle characteristics in the analyzed thunderstorms. These observed lifetimes and may differ from the real lifetimes. For example, a real short-lived thunderstorm was detected for 15 min. After 15 min the thunderstorm is detected for the last time, since the strong updraft diminishes. If any clouds exists at the presumed position afterwards (e.g. an anvil), a maximum of 60 min is added to the detected lifetime. Consequently, an isolated cell detected for 15 min will have a lifetime of 75 min in the analysis. If the anvil lifetime exceeds 60 min, it will not be considered in the life cycle of the analyzed thunderstorms.

The average evolution of $BT_{\min}$ and of $A_{\tau>0.1}$ show the strongest typical signatures of the analyzed data set during the lifetime progress compared to the other analyzed parameters. Therefore, they are chosen to define the life cycle phases (see Figure 4). The *early growth* (phase I) is defined from 30 min before the first satellite based detection up to the moment when the cooling trend of $BT_{\min}$ reaches its maximum indicating a rapid vertical cloud growth. The *advanced growth* (phase II) lasts until the cooling stops. This phase shows further vertical cloud growth until the maximum height is reached, for example, at the tropopause. The *maturity* (phase III) is defined as the time from stop of cooling until the time the maximum A_{cb} decrease is reached. This strong decrease marks the beginning of the last phase, the *decay* (phase IV). This life cycle definition follows the main life cycle stage characteristics of isolated single cells defined by Mecikalski et al. (2012). Although these life cycle phases are derived from an average over a multitude of different thunderstorm organziation types, they show similar characteristics as life

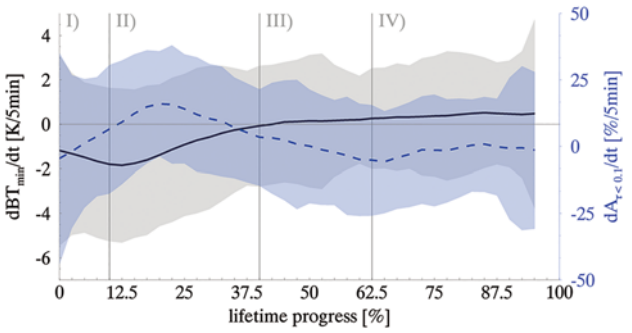

Figure 4: Mean trend and the standard deviation of minimum brightness temperature ($BT_{\min}$) in Kelvin per 5 min period (black line and greyish area) and of the area inside A_{cb} where $\tau > 0.1$ ($A_{\tau>0.1}$) in percent over 5 min (dashed blue line and bluish area) of all thunderstorms normalized to their lifetime and separated into the life cycle phases *early growth* (I), *advanced growth* (II), *maturity* (III), and *decay* (IV).

cycle definitions for single cells (e.g., Byers and Braham Jr., 1948; Mecikalski et al., 2012). However, the standard deviation (greyish and blueish area in Figure 4) is large compared to the characteristics due to the consideration of several organization types and as a consequence of merging and splitting cells' incomplete life cycles.

3.3.1 Early growth

In the following, the behavior of all parameters during the identified life cycle phases for short-, medium- and long-lived thunderstorms is investigated and described in detail.

In the analyzed data set this first phase of the medium-lived thunderstorm is represented by a steady decrease of satellite observed $BT_{\min}$ (Figure 5, dashed green line). At the beginning $BT_{\min}$ has a mean value of 236 K over all medium-lived thunderstorm events. It decreases with about −1 K/5 min indicating the vertical growth driven by an intensifying updraft due to strong condensation (Doswell III, 1987). The standard deviation (greenish area in Figure 5) covers the values of 225 K to 250 K. Despite the large range the decrease of BT can still be detected during this phase. The cloud area $A_{\tau>0.1}$ shows low values ($\approx$ 200 km^2) and no change during this phase (also in the standard deviation). No horizontal expansion is detected, since the primary cloud growth is a vertical in this phase. Optical thickness τ and cloud particle size r_e are both increasing during this phase. The parameter τ increases due to the vertical growth (compare to Mecikalski et al., 2011). The increase of r_e indicates the particle growth on the basis of condensation and coalescence. The cloud top *ice fraction* starts at mean values of 85 % as a mixed value between liquid and ice. Then it increases further towards complete glaciation (Figure 6), since the cloud top reaches heights where temperatures are low enough for all cloud droplets to freeze. The standard deviation covers values between 50 to 100 %. The radar parameters $R_{\max}$ and $VIL_{\max}$ show an increase and also indicate growing cloud particle size. $VIL_{\max}$ values are relatively low compared to existing literature (Amburn and Wolf, 1997). This can be traced back to the calculation and allocation of the parameters for a Cb-TRAM object. The consideration of 10 % of the detected radar echo region inside each thunderstorm is still large compared to the compact regions of maximum $VIL_{\max}$ occurrence. Thus maximum values are smoothed out. In the early growth phase hardly any lightning is observed, because in this phase updrafts are not strong enough for necessary friction induced charge separation as described in Feynman et al. (1964). Rigo et al. (2010) analyzed the life cycle of thunderstorms over Spain and detected weak lightning activity in the early development also. The general picture provided is a thunderstorm system which mainly grows vertically with increasing droplet sizes and ongoing glaciation. Horizontal growth is not detected yet.

Differences between the lifetime classes short- (Figure 5 and 6, dotted line) and long-lived (Figure 5 and 6, solid line) are very systematic, since short-lived thunderstorms seem to be at a later development stage already when detected for the first time. It is most striking that short-lived thunderstorms start at higher heights (colder temperatures $BT_{\min}$) and have larger extent (larger $A_{\tau>0.1}$ and τ) than long-lived ones. In addition, cloud tops of the shortest-lived thunderstorms are already almost completely glaciated while longest-lived are observed as liquid clouds. The large values of r_e might hint at the presence of large particles from mixed phase and ice cloud processes. In many cases the short-lived class is obviously dominated by thunderstorms which develop from existing large scale cloudiness "out-of-sight" under existing high cloud cover, e.g., in a frontal environment. This is confirmed by the fact that the short-lived class shows lightning activity ($Li > 0$) already early in their life cycle (see Figure 6).

All parameters show a large standard deviation during this phase. This is a result of the consideration of incomplete life cycles as a consequence of thunderstorm splitting from existing well developed thunderstorms.

3.3.2 Advanced growth

In the observational data phase II of the medium-lived thunderstorm (Figure 5 and 6, dashed green line) is dominated by rising cloud top represented by decreasing $BT_{\min}$ as well as by beginning horizontal growth of the storm object ($A_{\tau>0.1}$) and increasing optical thickness τ. Machado et al. (1997) and Feng et al. (2012) also show a decreasing $BT_{\min}$ during growth of MCSs over America (tropical and mid latitude) and an increase in $A_{\tau>0.1}$. Most interestingly, effective radius values display a clear decrease of particle size r_e starting just from the beginning of this phase while the *ice fraction* shows progressing glaciation at the same time. The decrease of r_e is an

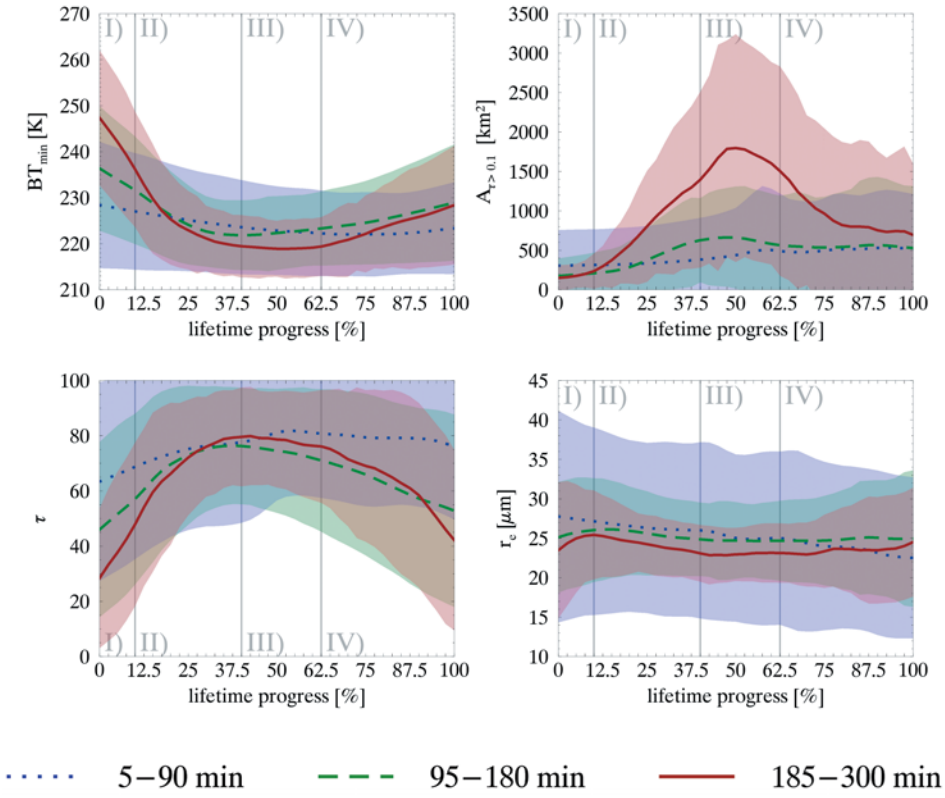

Figure 5: The lifetime classes short-lived (5–90 min, dotted blue line), medium-lived (95–180 min, dashed green line) and long-lived (185–300 min, solid red line) are normalized to the lifetime progress [%]. The parameters BT_{min} (top left), $A_{\tau>0.1}$ (top right), τ (bottom left) and r_e (bottom right) are depicted. The mean values and corresponding standard deviations over the life cycle are smoothed over three 5-minute time steps for visual clarity. The life cycle phases *early growth* (I), *advanced growth* (II), *maturity* (III), and *decay* (IV) are separated by vertical grey lines.

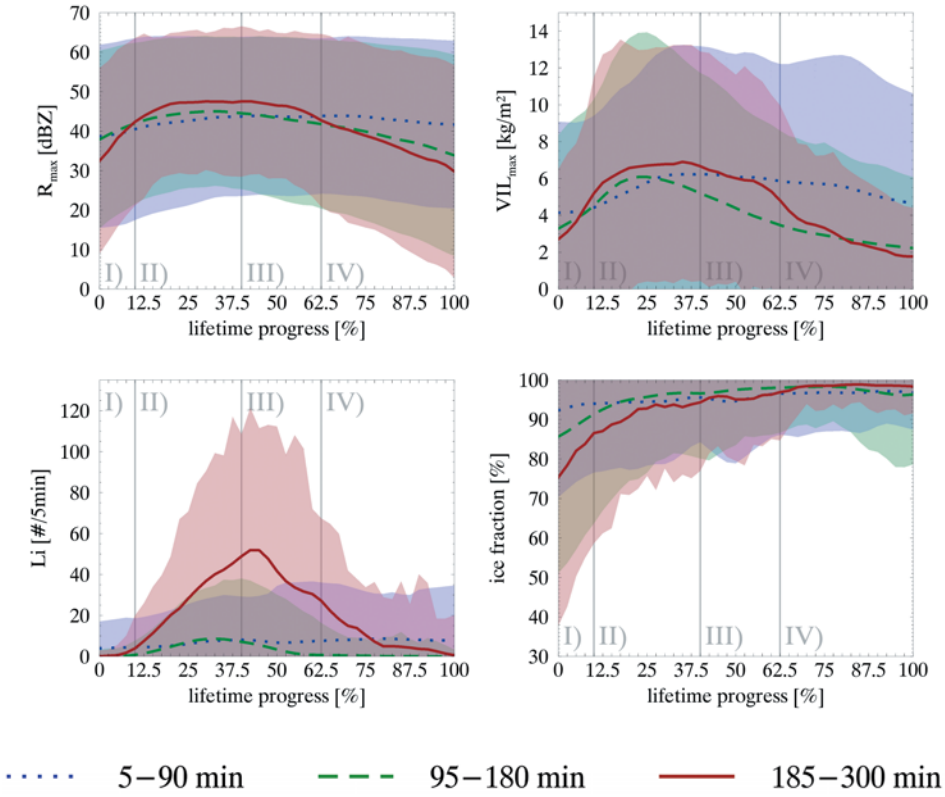

Figure 6: Like Figure 5. The parameters R_{max} (top left), VIL_{max} (top right), *Li* (bottom left) and *ice fraction* (bottom right) are depicted.

indicator for an intensifying updraft (Rosenfeld et al., 2008). This confirms the results of the study of Senf et al. (2015) where they analyzed convective growth and glaciation of thunderstorms over Central Europe based on radar data. Mecikalski et al. (2011) describe that a change from increasing r_e to decreasing when glaciation sets in. R_{max}, as a proxy of surface precipitation, slowly approaches a maximum mean value of about 45 dBZ. Davini et al. (2012) mention a maximum of reflectivity in the first half (growth phase) of a thunderstorm life cycle. Additionally VIL_{max} reaches its maximum and decreases afterwards. First lightning occurs and intensifies. In the study of Rigo et al. (2010), lightning activity starts with an increasing horizontal size of the thunderstorm. This result is also seen in the analyzed data since $A_{\tau>0.1}$ starts to increase at the beginning of phase II as well as *Li*. *Li* reaches its maximum value at the end of phase II. In general, the picture that is provided from the data set in phase II is that of an intensifying convective cloud system with further vertical growth, intensified mixed phase precipitation formation and related lightning activity as well as beginning horizontal divergence.

As far as differences between the lifetime classes short- (Figure 5 and 6, dotted blue line) and long-lived (Figure 5 and 6, solid red line) are concerned, the beginning of this phase is still influenced by the mentioned start of shorter life cycle observations from existing cloud systems for BT_{min} and τ. During phase II this behavior diminishes and long-lived objects start to show clear signs of stronger cooling trends related to more intense updraft, higher cloud top altitudes, larger area and higher lightning activity compared to short-lived ones. Differences for τ disappear during this phase as all values approach the maximum value of optical thickness retrievals. Over the full phase long-lived objects show smaller r_e than short-lived which could be related to new activation of ice nuclei in the stronger updrafts. The standard deviation of short-lived thunderstorms is very large compared to the standard deviation of the other lifetime classes for the parameter r_e. This supports the interpretation that this class contains a specifically wide mixture of cell types, real fresh developments as well as matured cells and secondary developments from splitting events. There are signs of higher values for VIL_{max} and R_{max} for long-lived objects. Davini et al. (2012) also find a positive correlation of reflectivity and lifetime of thunderstorms.

3.3.3 Maturity

Highest cloud tops, related to lowest BT_{min} values during the life cycle, are reached during this phase. Vertical and horizontal development stops and slowly changes to beginning decay. Matching these results Machado et al. (1997) showed that the values of BT_{min} reach their minimum in the end of the first half of their life cycle. The parameters $A_{\tau>0.1}$ and τ reach or stay close to their maximum and dissipate afterwards (as in Machado et al., 1997 and Rigo et al., 2010). The decreasing τ in connection with the low BT_{min} values and the slight increase of *ice fraction* (showing ongoing top glaciation) indicates that the thunderstorm starts to dissipate from the bottom to top. The height of the thunderstorm top stays nearly constant at low temperatures allowing further freezing of cloud droplets (Doswell III, 1987). The decrease of r_e ceases together with the updrafts. Precipitation (R_{max}) and VIL_{max} decrease. The decrease of R_{max} was also presented in Davini et al. (2012). *Li* starts to decrease in phase III of the medium-lived thunderstorm. At the end of phase III lightning activity stops. This behavior can also be seen in Rigo et al. (2010). In this phase the updrafts tend to disappear consistent with the system reaching its maximum horizontal extent. Slow sedimentation of (larger) cloud ice particles leads to decreasing thickness and coverage.

Long-lived thunderstorms reach lower minimum of BT_{min}, higher maximum of $A_{\tau>0.1}$, smaller r_e and higher *Li* than short-lived thunderstorms. Lower BT_{min} and larger $A_{\tau>0.1}$ for long-lived thunderstorms are consistent with the results of Machado et al. (1997). Higher *Li* values for longer-lived thunderstorms can be also found in Rigo et al. (2010). Smaller r_e might be an indicator for stronger updrafts (as described in Rosenfeld et al. (2008)) necessary for long-lived thunderstorms (Doswell III, 1987). The long-lived tend to show more intense precipitation as presented by the higher values of R_{max} (also present in Davini et al., 2012). The correlation of lifetime and size of $A_{\tau>0.1}$ once more hint towards an increasing share of well organized multi-cell systems (e.g., Höller, 1994; Markowski and Richardson, 2010).

3.3.4 Decay

This phase is characterized by a slow increase of 0.5 K/5 min in BT_{min}. The parameter τ decrease as a result of an ongoing dissolution of the thunderstorm cloud. $A_{\tau>0.1}$ stops to show clear changes, since the anvil is still detected. The precipitation as described by the parameter R_{max} (also seen in Davini et al., 2012) weakens and VIL_{max} decreases further. The parameter *ice fraction* almost reaches 100 %. A cloud system with a thinning cirrus anvil is observed. Almost all clouds within the considered cloud area are glaciated at their tops now. Hardly any liquid water at lower levels is observed anymore (as in Rigo et al., 2010). No lightning activity is detected anymore, since the updrafts have stopped (Doswell III, 1987).

With respect to the lifetime some differences can be detected in this phase. At the end of this phase the life cycle of the short-lived lifetime class is characterized by lower BT_{min}, $A_{\tau>0.1}$ and r_e values, and higher τ, R_{max}, VIL_{max} and *Li* values compared to the long-lived lifetime class. These tendencies are contrary to other studies (as for example, Davini et al., 2012; Machado et al., 1997) and are an indicator that the end of the life cycle of short-lived thunderstorms is marked by merging with other DMCs.

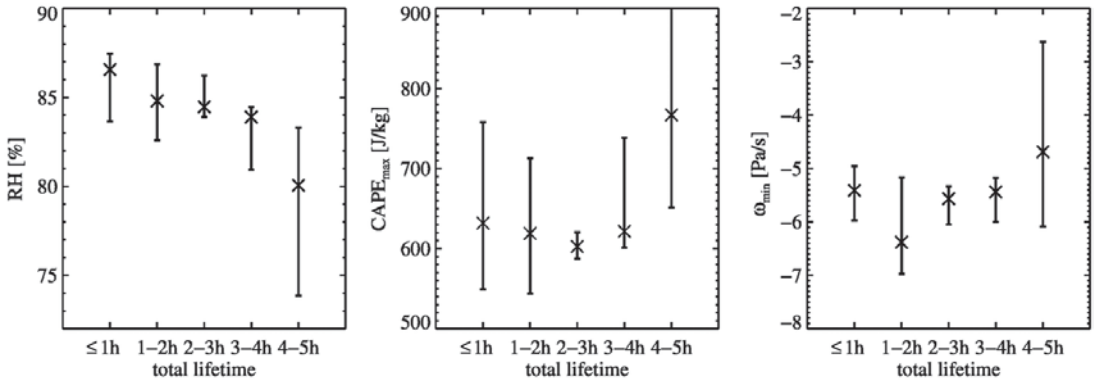

Figure 7: Median (x-symbol), 25th and 75th percentiles of the first life cycle time step of thunderstorms in June 2016, May, June, and July 2017, and June 2016 for the lifetimes ≤ 1 h, 1–2 h, 2–3 h, 3–4 h, 4–5 h for the model parameters relative humidity at 700 hPa (*RH*), maximum Convective Available Potential Energy ($CAPE_{max}$), and minimum vertical velocity at 700 hPa (ω_{min}).

3.4 The life cycle in NWP parameters

The environmental parameters $CAPE_{max}$, *RH*, and ω_{min} from the NWP model describe the convective environment, but cannot be interpreted down to the exact observed thunderstorm's position. Even worse, if convection is triggered in the model at the position of the observed storm, $CAPE_{max}$ will be strongly reduced and a misleading low convective potential would be diagnosed.

As a consequence of their consideration as non-local environmental information (averaged over a radius of 50 km at hourly availability), the model parameters do not show significant changes during individual life cycle phases. To evaluate whether or not indications for the lifetime at an early stage exist, the median of the model parameters and the 25th and 75th percentiles are calculated for the time of first detections of thunderstorms with a lifetime of ≤ 1 h (140 cases), 1–2 h (651 cases), 2–3 h (737 cases), 3–4 h (273 cases), and 4–5 h (58 cases) (see Figure 7). It turns out that the median of *RH* and $CAPE_{max}$ indicate differences between long-lived and short-lived DMCs. Short-lived thunderstorms seem to have higher *RH* and lower $CAPE_{max}$ at the beginning of their life-cycle. This tendency is still visible in the 25th/75th percentiles. This is especially obvious for long-lived thunderstorms with lifetimes of 4–5 hours which can be traced back to small numbers of thunderstorms in this lifetime bin. These results are in agreement with previous studies which have seen a similar behavior of $CAPE_{max}$ in several case studies (Rasmussen and Blanchard, 1998). In contrast, several studies showed that the reliability of a thunderstorm prediction based on $CAPE_{max}$ alone is weak (e.g. Wilson and Megenhardt, 1997; Tuovinen et al., 2015; Nguyen et al., 2020). Nevertheless, in this analysis the parameter $CAPE_{max}$ shows a slight predictive skill with larger values for very long-lived thunderstorms. In contrast to *RH* and lower $CAPE_{max}$, the parameter ω_{min} does not show a clear tendency. The ω_{min} values of long-lived thunderstorms with lifetimes of 4–5 hours seem to be higher than those of shorter-lived, but the 25th/75th show high variability and no clear tendency. Therefore, ω_{min} does not seem to be too suited as indicator for lifetime.

4 Summary and conclusions

The typical characteristics of parameters from satellite, radar, lightning, and numerical model data were investigated for an extensive data set of DMCs over Germany initially detected by the satellite-based tracking and nowcasting algorithm Cb-TRAM (Zinner et al., 2008; Zinner et al., 2013). The aim was the identification of relevant parameters with the skill to improve the nowcasting of thunderstorm lifetimes. Contrary to previous studies, the analysis was performed for the full mixture of observed DMC regardless of its organization type, since our focus is an operational forecasting environment where no simple method is available to differentiate organization types. Cb-TRAM detections for the months June 2016, May, June, July 2017, and June 2018 with almost 1900 DMCs observed over Germany were sorted by their lifetime between 5 min and 5 hours using 5-minute time intervals. More than half of the detected thunderstorm objects have a lifetime between 90–175 min. Short-lived objects (<90 min) are rare, partly due to missed early convection stages masked by cirrus clouds and due to the fact that multi cells with longer lifetimes are most frequent in Germany (for example, Wilson et al., 1998). In order to compare characteristics of the parameters for this variety of lifetimes, all lifetimes were normalized to a scale from 0 to 100 % where 0 represents the onset of convection corresponding to the first Cb-TRAM detection and 100 % represents the final decay corresponding to the last Cb-TRAM detection. The life cycle characteristics of the following lifetime classes were analyzed: short-lived (5–90 min), medium-lived (95–180 min) and long-lived (180–300 min). In summary, we came to the following answers of the questions from Section 3.

1. *Which parameters contain redundant information on the life cycle?*

   After correlation analyses the following observational parameters (containing different life cycle information) were selected to describe the typical characteristics: $BT_{\min}$, $A_{\tau>0.1}$, τ, r_e, *ice fraction*, $R_{\max}$, $VIL_{\max}$, and *Li*. These parameters and the model parameters $CAPE_{\max}$, *RH*, and $\omega_{\min}$ were examined over the normalized life cycle and are expected to represent the physical properties of the thunderstorm.

2. *Which parameters are able to describe certain life cycle phases, and what are their typical characteristics throughout each life cycle phases?*

   The trend of the parameters $BT_{\min}$ and $A_{\tau>0.1}$ are most suitable to classify the life cycle phases *early growth*, *advanced growth*, *maturity*, and *decay*. Although a large variety of different organization types and thunderstorm lifetimes were considered, all observational parameters still reflect lifetime characteristics comparable to single cell life cycle definitions Byers and Braham Jr. (1948). In the *early growth* a strong decrease of $BT_{\min}$ and an increase of τ, r_e, *ice fraction*, $R_{\max}$, and $VIL_{\max}$ can be observed. The *advanced growth* phase is characterized by an ongoing decrease in $BT_{\min}$ and increase in $A_{\tau>0.1}$, τ and *ice fraction*. The parameters r_e, $R_{\max}$, and $VIL_{\max}$ reach their maximum values. Lightning activity *Li* starts to increase and reaches its maximum at the end of this phase. At the beginning of the *maturity* phase the parameter $BT_{\min}$ reaches its minimum, $A_{\tau>0.1}$ its maximum, $R_{\max}$, and $VIL_{\max}$ decrease. The *decay* phase is characterized by an increasing $BT_{\min}$ and decreasing $R_{\max}$ and $VIL_{\max}$. In the second half of the *decay* phase lightning activity stops.

3. *Are there differences in the life cycle between long-lived and short-lived thunderstorms?*

   Differences between different lifetimes were found. In general, life cycle characteristics were not as pronounced in the short-lived thunderstorms than in the long-lived ones. Long-lived thunderstorms, on average, showed higher maximum values of $A_{\tau>0.1}$, *Li*, and $VIL_{\max}$ than short-lived thunderstorms during *advanced growth* and *maturity*. In addition, short-lived thunderstorms usually begin at lower $BT_{\min}$ values and higher τ values than long-lived thunderstorms. However, this is a result that can only be attributed to the fact that some thunderstorms cannot be detected by Cb-TRAM before they have reached some characteristic intensity. Consequently, the characteristics for short- and long-lived thunderstorms are highly dependent on the satellite detection based separation of thunderstorms used here. Nevertheless, these results can be used for a nowcasting based on Cb-TRAM detections. As already described by Sun et al. (2014) we also find that NWP model parameters do not show any significant change during life cycle phases, because the model prediction is not specific in time and space down to individual thunderstorm level. However, they do show general differences at the time of the onset of convection (first detection in satellite data) for long- cpmpared to short-lived thunderstorms in a larger environment context. For a 50 km environment around the thunderstorm, the parameter $CAPE_{\max}$ seems to be lower and *RH* higher for short-lived objects compared to long-lived ones. Due to their large variability the model parameters should only be used for the lifetime nowcasting in connection with observational data.

These results carry large standard deviations. In part this reflects the statistical nature of turbulent convection. In part it is result of our missing separation of thunderstorm types, since the aim of this study is to find parameters that show signatures for lifetime prediction in an operationally available thunderstorm detection algorithm.

For the future it would be interesting whether other NWP parameters would show more robust signatures. The 0–6 km wind shear was analyzed as well, but similarly to $\omega_{\min}$ no lifetime of life cycle characteristics could be identified. This result is in contrast to the results of Markowski and Richardson (2010). One reason for this might be the incomplete life cycles due to higher cloud cover or splitting event in operational data and their effect on the observed statistics. Another reason is the limited temporal and spatial resolution resulting in a time/space shift of the signatures. In addition, IC and CG lightning could be analyzed separately. Rigo et al. (2010) showed that slight differences in frequency and initial time exist.

The results of this study are foreseen to be used as basis for a subsequent implementation in a life cycle model for an identification of current life cycle stage and an improved nowcasting of remaining lifetime of DMCs. There the significant characteristics of the thunderstorm's lifetime presented in the analyzed parameters will be combined with a fuzzy logic based approach (based on Zadeh, 1965).

Acknowledgments

This research is funded by the DWD Extramural Research (EMF) program. We are grateful to the nowcast GmbH for providing the lightning data and to EUMETSAT for providing the Meteosat data. Meteosat data are copyrighted by EUMETSAT.

Acronyms

A_{cb}	area of the Cb-TRAM cell
$A_{\tau>0.1}$	area inside A_{cb} where $\tau > 0.1$
APICS	Algorithm for the Physical Investigation of Clouds with SEVIRI
BT	brightness temperature

$BT_{\min}$	minimum brightness temperature
CAPE	Convective Available Potential Energy
$CAPE_{\max}$	maximum Convective Available Potential Energy
Cb-TRAM	Cumulonimbus Tracking And Monitoring
CG	cloud-to-ground
COCS	cirrus optical properties derived from CALIOP and SEVIRI algorithm during day and night
COSMO-D2	COnsortium for Small scale MOdeling with a grid spacing of 2.2 km has been operated since May 2018
COSMO-DE	COnsortium for Small scale MOdeling with a grid spacing of 2.8 km operated until May 2018
DLR	Deutsches Zentrum für Luft- und Raumfahrt e. V.
DWD	Deutscher Wetterdienst
HRV	High Resolution Visible channel
IC	Intra Cloud
IR	Infra-Red channel
Li	lightning detection
LINET	European ground-based Lightning Network
NWP	Numerical Weather Prediction
ω	vertical velocity at 700 hPa
$\omega_{\min}$	minimum vertical velocity at 700 hPa
ice fraction	ice fraction at the cloud top
r_e	effective radius
$R_{\max}$	maximum reflectivity
RA_{46}	area of the 46 dBZ contour
Rad-TRAM	Radar Tracking and Monitoring *RH* relative humidity at 700 hPa
SEVIRI	Spinning Enhanced Visible and Infra-Red Imager
τ	cloud optical thickness
VII	vertically integrated ice content
$VII_{\max}$	maximum vertically integrated ice content
VIL	vertically integrated liquid water content
$VIL_{\max}$	maximum vertically integrated liquid water content
VIS	visible channel
WV	water vapor channel

References

Amburn, S.A., P.L. Wolf, 1997: VIL density as a hail indicator. – Wea. Forecast. **12**, 473–478 DOI: 10.1175/1520-0434(1997)012<0473:VDAAHI>2.0.CO;2.

Baldauf, M., K. Stephan, S. Klink, C. Schraff, A. Seifert, J. Förstner, T. Reinhardt, C.J. Lenz, 2006: The new very short range forecast model LMK for the convection-resolving scale. – Second THORPEX International Science Symposium. Volume of extended abstracts Part B, 148–149.

Benjamin, S.G., B.E. Schwartz, E.J. Szoke, S.E. Koch, 2004: The value of wind profiler data in u.s. weather forecasting. – BAMS **85**, 1871–1886. DOI: 10.1175/BAMS-85-12-1871.

Betz, H.D., K. Schmidt, P. Laroche, P. Blanchet, W.P. Oettinger, E. Defer, Z. Dziewit, J. Konarski, 2009: LINET – An international lightning detection network in Europe. – Atmos. Res. **91**, 564–573. DOI: 10.1016/j.atmosres.2008.06.012.

Brooks, H., N. Dotzek, 2008: The spatial distribution of severe convective storms and an analysis of their secular changes. – Climate Extremes and Society, 35–53. DOI: 10.1017/CBO9780511535840.

Bugliaro, L., T. Zinner, C. Keil, B. Mayer, R. Hollmann, M. Reuter, W. Thomas, 2011: Validation of cloud property retrievals with simulated satellite radiances: a case study for SEVIRI. – Atmos. Chem. Phys. **11**, 5606–5624. DOI: 10.5194/acp-11-5603-2011.

Byers, H.R., R.R. Braham Jr., 1948: Thunderstorm structure and circulation. – J. Meteor. **5**, 71–86. DOI: 10.1175/1520-0469(1948)005<0071:TSAC>2.0.CO;2.

Cintineo, J.L., M.J. Pavolonis, J.M. Sieglaff, A.K. Heidinger, 2013: Evolution of severe and nonsevere convection inferred from GOES-derived cloud properties. – J. Appl. Meteor. Climatol. **52**, 2009–2023. DOI: 10.1175/JAMC-D-12-0330.1.

Cintineo, R.M., M.J. Pavolonis, J.M. Sieglaff, D.T. Lindsey, G.L. Cronce, B.B. Rodenkirch, C. Gravelle, 2018: The NOAA/CIMS ProbSevere model: Incorporation of total lightning and validation. – Wea. Forecast. **33**, 331–345. DOI: 10.1175/WAF-D-17-0099.1.

Davini, P., R. Bechini, R. Cremonini, C. Cassardo, 2012: Radar-based analysis of convective storms over northwestern Italy. – Atmosphere **3**, 33–58. DOI: 10.3390/atmos3010033.

Doswell III, C.A., 1987: The destinction between large-scale an mesoscale contribution to severe convection: A case study example. – Wea. Forecast. **2**, 3–16. DOI: 10.1175/1520-0434(1987)002<0003:TDBLSA>2.0.CO;2.

Emanuel, K.A., 1994: Atmospheric Convection. – Oxford Press.

Farnell, C., T. Rigo, N. Pineda, 2017: Lightning jump as a nowcast predictor: Application to severe weather events in Catalonia. – Atmos. Res. **183**, 130–141. DOI: 10.1016/j.atmosres.2016.08.021.

Feng, Z., X. dong, B. Xi, S.A. McFarlane, A. Kennedy, B. Ling, P. Minnis, 2012: Life cycle of midlatitude deep convective systems in a Lagrangian framework. – J. Geophys. Res. **117**, D23. DOI: 10.1029/2012JD018362.

Feynman, R.P., R.B. Leighton, M. Sands, 1964: Electricity in the atmosphere. The Feynman Lectures on Physics. Vol. II: Mainly Electromagnetism and Matter. – – Addison-Wesley, Reading, MA 11 pp.

Fiolleau, T., R. Roca, 2013: An algorithm for the detection and tracking of tropical mesoscale convective systems using infrared images from geostationary satellite. – IEEE Trans Actions on Geoscience and Remote Sensing **51**, 4302–4315.

Greene, D.R., R.A. Clark, 1972: Vertically integrated liquid water – A new analysis tool. –

Mon. Wea. Rev. **100**, 548–552. DOI: 10.1175/1520-0493(1972)100<0548:VILWNA>2.3.CO;2.

Guillou, Y., 2010: Algorithm theoretical basis document for "rapid development thunderstorms". – Available online at http://www.nwcsaf.org/.

Hagen, M., U. Finke, 1999: Motion characteristics of thunderstorms in southern Germany. – Meteor. Applicat. **6**, 227–239. DOI: 10.1017/S1350482799001164.

Hansen, J.E., L.D. Travis, 1974: Light scattering in planetary atmospheres. – Space Sci. Rev. **16**, 527–610. DOI: 10.1007/BF00168069.

Hartung, D.C., J.M. Sieglaff, L.M. Cronce, W.F. Feltz, 2013: An intercomparison of UW Cloud-Top Cooling Rates with WSR-88D Radar Data. – Wea. Forecas. **28**, 463–480. DOI: 10.1175/WAF-D-12-00021.1.

Helmert, K., P. Tracksdorf, J. Steinert, M. Werner, M. Frech, N. Rathmann, T. Hengstebeck, M. Mott, S. Schumann, T. Mammen, 2014: DWDs new radar network and post-processing algorithm chain. – Proc. Eighth European Conf. on Radar in Meteorology and Hydrology. – Available online at http://www.pa.op.dlr.de/erad2014/programme/ExtendedAbstracts/237_Helmert.pdf.

Höller, H., 1994: Mesoscale organization and hailfall characteristics of deep convection in southern Germany. – Beiträge zu Physik der Atmosphäre – Contributions to Atmospheric Physics **67**, 219–234. – Available online at http://elib.dlr.de/31866/1/94-hoeller.pdf.

James, P.M., B.K. Reichert, D. Heizenreder, 2018: NowCastMIX: Automatic integrated warnings for severe convection on nowcasting time scales at the German Weather Service. – Wea. Forecast. **3**, 413–433. DOI: 10.1175/WAF-D-18-0038.1.

Jurković, P.M., N.S. Mahović, D. Počakal, 2015: Lightning, overshooting top and hail characteristics for strong convective storms in Central Europe. – Atmos. Res. **161-162**, 153–168. http://www.sciencedirect.com/science/article/pii/S0169809515001155.

Kahraman, A., M. Kadiglu, P. Markowski, 2017: Severe convective storm environments in Turkey. – Mon. Wea. Rev. **145**, 4711–4725. DOI: 10.1175/MWR-D-16-0338.1.

Kaltenböck, R., G. Diendorfer, N. Dotzek, 2009: Evalutation of thunderstorm indices from ECMWF analyses, lightning data and severe storm reports. – Atmo. Res. **93**, 381–396. DOI: 10.1016/j.atmosres.2008.11.005.

Kober, K., A. Tafferner, 2009: Tracking and nowcasting of convective cells using remote sensing data from radar and satellite. – Meteorologische Zeitschrift **18**, 75–84. DOI: 10.1127/0941-2948/2009/359.

Kox, S., L. Bugliaro, A. Ostler, 2014: Retrieval of cirrus cloud optical thickness and top altitude from geosationary remote sensing. – Atmos. Meas. Tech. **7**, 3233–3246. DOI: 10.5194/amt-7-3233-2014.

Kuligowski, R.J., A.P. Barros, 1998: Localized precipitation forecasts from a numerical weather prediction model using artifical neural networks. – Wea. Forecast. **13**, 1194–1204. DOI: 10.1175/1520-0434(1998)013<1194:LPFFAN>2.0.CO;2.

Machado, L.A.T., W.B. Rossow, R.L. Guedes, A.W. Walker, 1997: Life cycle variations of mesoscale convective systems over the Americas. – Mon. Wea. Rev. **126**, 1630–1654. DOI: 10.1175/1520-0493(1998)126<1630:LCVOMC>2.0.CO;2.

Markowski, P., Y. Richardson, 2010: Mesoscale meteorology in midlatitudes. – John Wiley & Sons.

Mathon, V., H. Laurent, 2001: Life cycle of Sahelian mesoscale convective cloud systems. – Quarterly Journal of the Royal Meteorological Society **127**, 377–406. DOI: 10.1002/qj.49712757208.

Mattos, E.V., L.A.T. Machado, 2011: Cloud-to-ground lightning and mesoscale convective systems. – Atmos. Res. **99**, 377–390. DOI: 10.1016/j.atmosres.2010.11.007.

Mecikalski, J., K.M. Bedka, 2006: Forecasting Convective Initiation by Monitoring the Evolution of Moving Cumulus in Daytime GOES Imagery.. – Mon. Wea. Rev. **134**, 49–78. DOI: 10.1175/MWR3062.1.

Mecikalski, J., P.D. Watts, M. König, 2011: Use of Meteosat Second Generation optimal cloud analysis field for understanding physical attributes of growing cumulus clouds. – Atmos. Res. **102**, 175–190. DOI: 10.1016/j.atmosres.2011.06.023.

Mecikalski, J., K. Bedka, M. König, 2012: Best practice document. – EUMETSAT Convection Working Group **Version 2.0**.

Mecikalski, J., D. Rosenfeld, A. Manzato, 2016: Evaluation of geostationary satellite observations and the development of a 1–2 h prediction model for future storm intensity. – J. Geophys. Res. Atmos. **121**, 6374–6392. DOI:10.1002/2016JD024768.

Meyer, V., H. Höller, H. Betz, 2013: Automated thunderstorm tracking: Utilization of three-dimensional lightning and radar data. – Atmos. Chem. Phys. **13**, 5137–5150. DOI: 10.5194/acp-13-5137-2013.

Nakajima, T., M.D. King, 1990: Determination of the optical thickness and effective particle radius of clouds from reflected solar radiation measurements. Part I: Theory. – J. Atmos. Sci. **47**, 1878–1893. DOI: 10.1175/1520-0469(1990)047<1878:DOTOTA>2.0.CO;2.

Nguyen, L., M. Rohrer, M. Schwarb, M. Stoffel, 2020: Development of a combined empirical index for a 5-day forecast of heavy precipitation over the Bernese Alps. – Env. International **135**, 105357. DOI: 10.1016/j.envint.2019.105357.

Nisi, L., P. Ambrosetti, L. Clementi, 2014: Nowcasting severe convection in the Alpine region: the COALITION approach. – Quart. J. Roy. Meteor. Soc. **140**, 1684–1699. DOI: 10.1002/qj.2249.

Rasmussen, E.N., D.O. Blanchard, 1998: A baseline climatology of sounding-derived supercell and tornado forecast parameters. – Wea. Forecast. **13**, 1148–1164. DOI: 10.1175/1520-0434(1998)013<1148:ABCOSD>2.0.CO;2.

Rigo, T., N. Pineda, J. Bech, 2010: Analysis of warm season thunderstorms using an object-oriented tracking method based on radar and total lightning data. – Nat Hazard Earth Sys. **10**, 1881–1893. DOI: 10.5194/nhess-10-1881-2010.

Roberts, R.D., S. Rutledge, 2003: Nowcasting storm initiation and growth using GOES-8 and WSR-88D data. – Wea. Forecast. **18**, 562–584. DOI: 10.1175/1520-0434(2003)018<0562:NSIAGU>2.0.CO;2.

Rosenfeld, D., W.L. Woodley, A. Lerner, G. Kelman, 2008: Satellite detection of severe convective storms by their retrieved vertical profiles of cloud particle effective radius and thermodynamic phase. – J. Geophys. Res. **113**, D04208. DOI: 10.1029/2007JD008600.

Schmetz, J., P. Pili, S. Tjemkes, D. Just, J. Kerkmann, S. Rota, A. Ratier, 2002: An introduction to Meteosat Second Generation (MSG). – Bull. Amer. Meteor. Soc. **83**, 977–992. DOI: 10.1175/1520-0477(2002)083<0977:AITMSG>2.3.CO;2.

Schultz, C.J., W.A. Petersen, L.D. Carey, 2009: Preliminary development and evaluation of lightning jump algorithms for the real-time detection of severe weather. – J. Appl. Meteor. Climatol. **48**, 2543–2563. DOI: 10.1175/2009JAMC2237.1.

Schultz, C.J., W.A. Petersen, L.D. Carey, 2011: Lightning and severe weather: A comparison between total anc cloud-to-ground lightning trends. – Wea. Forecast. **26**, 744–755. DOI: 10.1175/WAF-D-10-05026.1.

Senf, F., H. Deneke, 2017: Satellite-based characterization of convective growth and glaciation and its relationship to precipitation formation over Central Europe. – J. Appl. Meteor. Climatol. **56**, 1827–1845. DOI: 10.1175/JAMC-D-16-0293.1.

Senf, F., F. Dietzsch, A. Huenerbein, H. Deneke, 2015: Characterization of initiation and growth of selected severe convective storms over Central Europe with MSG-SEVIRI. – J. Appl. Meteor. Climatol. **54**, 207–224. DOI: 10.1175/JAMC-D-14-0144.1.

Setvák, M., C.A. Doswell, 1991: The AVHRR Channel 3 Cloud Top Reflectivity of Convective Storms. – Mon. Wea. Rev. **119**, 841–847. DOI: 10.1175/1520-0493(1991)119<0841:TACCTR>2.0.CO;2.

Strandgren, J., L. Bugliaro, 2018: The life cycle of anvil cirrus clouds from geostationary satellite remote sensing. – AGU Fall Meeting Abstracts, A11J–2366. https://ui.adsabs.havard.edu/abs/2018AGUFM.A11J2366S.

Sun, J., M. Xue, J.W. Wilson, I. Zawadzki, S.P. Ballard, J. Onvlee-Hooimeyer, P. Joe, D.M. Barker, P. Li, B. Golding, M. Xu, J. Pinto, 2014: Use of NWP for nowcasting convective precipitation: Recent progress and challenges. – Bull. Amer. Meteor. **95**, 209–426. DOI: 10.1175/BAMS-D-11-00263.1.

Taszarek, M., J. Allen, T. Pucik, P. Groenemeijer, B. Czernecki, L. Kolendowicz, K. Lagouvardos, V. Kotroni, W. Schulz, 2019: A climatology of thunderstorms across Europe from a synthesis of multiple data sources. – J. Climate **32**, 1813–1837. DOI: 10.1175/JCLI-D-18-0372.1.

Tuovinen, J., J. Rauhala, D.M. Schultz, 2015: Significant-hail-producing storms in Finland: Convective-storm environment and mode. – Wea. Forecast. **30**, 1064–1076. DOI: 10.1175/WAF-D-14-00159.1.

Waldvogel, A., B. Federer, P. Grimm, 1979: Criteria for the detection of hail cells. – J. Appl. Meteor. **18**, 1521–1525. DOI: 10.1175/1520-0450(1979)018<1521:CFTDOH>2.0.CO;2.

Wang, Y., E.D. Coning, A. Harou, W. Jacobs, P. Joe, L. Nitina, R. Roberts, J. Wang, J. Wison, A. Atenica, B. Bica, B. Brown, S. Goodmann, A. Kann, P.W. Li, I. Monteiro, P. Parrish, F. Schmid, A. Seed, J. Sun, 2017: Guidelines for nowcasting techniques. – https://library.wmo.int/doc_num.php?explnum_id=3795.

Wapler, K., 2013: High-resolution climatology of lightning characteristics within Central Europe. – Meteor. Atmos. Phys. **122**, 175–184. DOI: 10.1007/s00703-013-0285-1.

Wapler, K., 2017: The life-cycle of hailstorms: Lightning, radar reflectivity and rotation characteristics. – Atmos. Res. **193**, 60–72. DOI: 10.1016/j.atmosres.2017.04.009.

Wapler, K., submitted: Mesocyclonic and non-mesocyclonic convective storms in Germany: Storm characteristics and life-cycle. – Atmos Res.

Wilson, J.W., D.L. Megenhardt, 1997: Thunderstorm initiation, organization, and lifetime associated with Florida boundary layer convergence lines. – Mon. Wea. Rev. **125**, 1507–1525. DOI: 10.1175/1520-0493(1997)125<1507:TIOALA>2.0.CO;2.

Wilson, J.W., N.A. Crook, C.K. Mueller, J. Sun, M. Dixon, 1998: Nowcasting thunderstorms: A status report. – Bull. Amer. Meteor. Soc. **79**, 2079–2099. DOI: 10.1175/1520-0477.

Zadeh, L.A., 1965: Fuzzy sets. – Information and control **8**, 338–353. DOI: 10.1016/S0019-9958(65)90241-X.

Zinner, T., H. Mannstein, A. Tafferner, 2008: Cb-TRAM: Tracking and monitoring severe convection from onset over rapid development to mature phase using multi-channel Meteosat-8 SEVIRI data. – Meteor. Atmos. Phys.**101**, 191–210. DOI: 10.1007/s00703-008-0290-y.

Zinner, T., C. Forster, de E. Coning, H.D. Betz, 2013: Validation of Meteosat storm detection and nowcasting system Cb-TRAM with lightning network data - Europe and South Africa. – Atmos. Mea. Tech. **6**, 1567–1585. DOI: 10.5194/amt-6-1567-2013.